Geomorphology 351 (2020) 106945

Contents lists available at ScienceDirect

Geomorphology

journal homepage: www.elsevier.com/locate/geomorph

Characterizing braided rivers in two nested watersheds in the Source Region of the Yangtze River on the Qinghai-Tibet Plateau

Zhiwei Li [a], Hanyou Lu [b], Peng Gao [c,*], Yuchi You [b], Xuyue Hu [b]

[a] State Key Laboratory of Water Resources and Hydropower Engineering Science, Wuhan University, Wuhan 430072, China
[b] Key Laboratory of Water-Sediment Sciences and Water Disaster Prevention of Hunan Province, Changsha University of Science & Technology, Changsha 410114, China
[c] Department of Geography, Syracuse University, Syracuse, New York 13244, USA

ARTICLE INFO

Article history:
Received 4 September 2019
Received in revised form 2 November 2019
Accepted 4 November 2019
Available online 11 November 2019

Keywords:
Braided river
Braiding intensity
Active valley width
Water discharge
Morphological change

ABSTRACT

Large and complex braided channels (>1 km wide) in the Source Region of the Yangtze River (SRYR) on the Qinghai-Tibet Plateau, China, are characterized by a unique alpine environment with very high elevations and glacier sources. Yet, little is known about the morphological complexity and changes of large braided channels owing to the scarcity of hydrological and topographical data. In this study, we provided the first insight into these issues using compiled long-term (several decades) climatic and suspended sediment data, and Landsat images of braided channels in two nested headwater watersheds (i.e., Tuotuo and Tongtian river watersheds) in the SRYR. Analysis of annual and monthly mean temperature, precipitation, and water discharges illustrated the nature of the hydrological regime and their response to glacier melting in the two watersheds. Examination of annual mean suspended sediment loads and concentrations (C) led to two sediment rating curves and generally similar C values between the two watersheds. Among a suite of morphological indices for braided rivers, braiding intensity may be quantified using four different ones. After comparing the indices, we showed that they had similar ability of characterizing braiding patterns and adopted branch count index (BI_{T3}) for further analysis. We found that BI_{T3} was linearly correlated with active valley width (W_R) during both flood and dry seasons for the 17 selected braided reaches distributed within the two nested watersheds. In addition, braiding density, defined as the ratio of BI_{T3} to W_R, remained approximately unchanged irrespective of elevations and locations of these reaches, indicating clearly that morphological structures of braided channels are spatially uniform in the SRYR. Along the main channels of the two nested watersheds over the entire study period, BI_{T3} always reached the maximum as R_W, defined as the ratio of water body to exposed active riverbed area, was around 0.43. Furthermore, R_W was always positively correlated with the associated water discharge (Q). Variable degrees of braiding adjustment in response to changes of hydrological regime were represented by hysteresis loops between BI_{T3} and Q. These results revealed relatively homogeneous morphologic properties of braided channels across the two nested watersheds and provided an important benchmark for future morphodynamic research on braided rivers in the SRYR.

1. Introduction

Braided rivers are generally developed in wide valleys with relatively steep slopes, abundant coarse sediment supply, and limited vegetation coverage (Ashmore, 1991; Bertoldi and Tubino, 2007; Nicholas, 2013; Chalov and Alexeevsky, 2015; Peirce et al., 2018). Multi-thread channels separated by irregular central bars or islands, are usually unstable at the intra- and inter-annual scales, and their bar dynamics and stability in some cases are significantly affected by riparian vegetation typically found in small-sized braided rivers (Ashmore, 1991; Gran and Paola, 2001; Coulthard, 2005; Bertoldi and Tubino, 2007; Tal and Paola, 2010; Bertoldi et al., 2011; Nicholas, 2013; Chalov and Alexeevsky, 2015; Gran et al., 2015; Peirce et al., 2018). Braided rivers may be found in various alluvial environments around the world, such as alluvial plains (e.g., the Lower Yellow River, the Indus River, and the Brahmaputra River) (Xu, 1997; Sarma, 2005; Dubey et al., 2014; Marra et al., 2014; Li et al., 2017a; An et al., 2018; Carling et al., 2018; Gogoi, 2018), semi-arid and arid environments (e.g., the Tarim River) (Storz-Peretz et al., 2016; Yu et al., 2016; Yu et al., 2017; Guerit et al., 2018; Schuurman et al., 2018), the North American Plain (e.g., the Saskatchewan and Sunwapta rivers) (Sambrook Smith et al., 2006; Unsworth et al., 2016; Middleton et al., 2018), the Tagliamento River in Italy (Bertoldi et al., 2009b; Bertoldi et al., 2010; Welber et al., 2012; Huber and Huggenberger, 2015; Surian and Fontana, 2017), the Rees River in New Zealand (Williams et al., 2015; Williams et al.,

* Corresponding author.
E-mail address: pegao@maxwell.syr.edu (P. Gao).

2016b), and on the Tianshan Mountain range and Qinghai-Tibet Plateau (QTP) (e.g., the source of Yangtze River, the source of Yellow River, the Upper Lancang River, and the Yarlung Tsangpo River basin) (Zhang, 1998; Karmaker and Dutta, 2011; Blue et al., 2013; Yu et al., 2013; Li et al., 2014; Li et al., 2016; Métivier et al., 2016; Li et al., 2017b; Wu et al., 2018b).

The planimetric characteristics and morphodynamic processes of braided rivers have attracted increasing attention from fluvial geomorphologists, sedimentologists, and river engineers in past decades because of growing demand for natural landscape tourism, riverine wetland protection, mineral resource development, and traffic engineering construction (Ashmore et al., 2011; Sun et al., 2015b; Redolfi et al., 2016; Connor-Streich et al., 2018; Peirce et al., 2018; Schuurman et al., 2018; Bakker et al., 2019). In braided channels, there are a variety of central bars, side bars, mid-channel bars, and islands of different sizes that lead to broken and scattered overall planimetrical morphology, so the branches, chutes, and lobes are randomly interlinked as confluence and bifurcation units. Building upon these variable patterns, strong intra- and inter-annual erosional and depositional processes occurring in flood and non-flood seasons enhance the variability of braided morphological characteristics (Bertoldi et al., 2009b; Bertoldi et al., 2009c; Schuurman et al., 2018). Furthermore, high sediment transport rates in flood seasons have significant impacts on morphological changes and the unstable dynamic status of braided channels. These complex interactions among flow, sediment, and morphology of braided rivers have been studied in terms of qualitative analysis (Sapozhnikov and Foufoula-Georgiou, 1996; Hundey and Ashmore, 2009; Ashmore et al., 2011), flume experiments (Bertoldi and Tubino, 2007; Egozi and Ashmore, 2009; Bertoldi et al., 2014; Javernick et al., 2018; Peirce et al., 2018), and morphodynamic modelling (Sun et al., 2015a; Schuurman et al., 2016; Williams et al., 2016a; Williams et al., 2016b; Schuurman et al., 2018).

Characterizing geometrics of braided channels is the key aspect of quantitative description of braiding features (Egozi and Ashmore, 2008; Hundey and Ashmore, 2009; Ashmore et al., 2011; Redolfi et al., 2016). Generally, braiding intensity is used to describe the degree of bifurcation a multi-thread channel system owing to separation of local bars and islands in braided channels. However, bifurcation is highly variable and interacts in complex ways with the braided channel network. As such, a variety of indices have been proposed to quantify the braiding intensity, such as the average number of braids (Howard et al., 1970), the bar length index (referring to the length and width of the bars and the frequency of occurrence) (Brice, 1960; Brice, 1964; Rust, 1972; Rust, 1978); the average number of branches in a given channel length (Howard et al., 1970; Ashmore, 1982) or the total length of branches in a given longitudinal river length (Ashmore, 1982; Friend and Sinha, 1993). These indices were obtained by calculating the number of branch or bar per cross section or the ratio of the total branch length to the entire channel length in a given reach, which was subsequently summarized and applied in flume experiments by Egozi and Ashmore (2008). While new methods of characterizing the morphological structure of braided rivers have been proposed continuously, such as using dimensionless discharge and stream power scaled by grain size and a representative length (Bertoldi et al., 2009c) or network analysis based on graph theory (Connor-Streich et al., 2018), no consensus has been reached on which index may be adopted for best characterizing the morphology of braided rivers. More exploration of these indices, particularly for large braided systems, is necessary.

However, calculating any index requires sufficient topographic data, which are often difficult to directly obtain from the field because of practical challenges in instruments, time, and costs (Wheaton et al., 2013; Williams et al., 2014; Williams et al., 2015). In recent years, aerial surveys using an Unmanned Aerial Vehicle (UAV) have been widely applied for obtaining high-resolution morphologic and topographic data of braided rivers (Cook, 2017; Pearson et al., 2017; Vázquez-Tarrío et al., 2017; Rusnák et al., 2018). Nonetheless, these data cover very limited time periods and thus have to give way to multi-source and multi-period remote sensing imagery to facilitate understanding of historical changes of morphology of braided rivers (Werbylo et al., 2017; Wu et al., 2018b; Fryirs et al., 2019). Thus far, analyzing morphological characteristics of braided rivers and their temporal changes have been performed in many low-elevation regions (Zanoni et al., 2008; Baki and Gan, 2012; Nicholas, 2013). In the remote Source Region of the Yangtze River (SRYR) in China, many large braided rivers exist that have developed wide braid-plains (typically 1–3 km) at very high elevations (Yu et al., 2014; Wang et al., 2016). Although these braided rivers have developed in unique high-elevation environments and played an important role in maintaining the health of the regional ecosystem, little is known about their morphological features and external controls.

To fill this gap, this study aims to (i) compare the differences of meteorological and hydrological factors of the two nested watersheds, (ii) quantitatively characterize and compare morphological structures of 17 selected braided reaches distributed across the two watersheds and 3 reaches along the main channel of each nested watershed, and (iii) quantitatively examine morphological responses of these braided reaches to variable flow regimes. Our results will provide first-hand scientific information to aid the development of best management practices for protecting braided riverine wetlands in the SRYR affected by overstocking, local engineering construction, and increased runoff variation induced by climate change.

2. Materials and methodology

2.1. Study area and data sources

The SRYR is situated in the hinterland of the Qinghai-Tibet Plateau (QTP). Its geographical scope is roughly between 32°30′~35°35′ N, 90°43′~96°45′ E, with an average elevation of 4500 m a.s.l., and a drainage area of approximately 1.401×10^5 km^2. The entire SRYR forms a watershed that contains a complex stream network with the Tongtian River as the main channel (Fig. 1a). In addition to >200 relatively small tributaries, it consists of three main sub-watersheds: the Tuotuo, the Dangqu, and the Chumaer River sub-watersheds. The main channel of the Tuotuo River sub-watershed is originated from glaciers near top of the Tanggula Mountain Range. In the Dangqu River sub-watershed, its main channel and the two major tributaries (i.e., the Gaerqu and Buqu rivers) are all derived from glaciers. The Dangqu River becomes the Tongtian River downstream from the confluence of the Gaerqu and Buqu rivers. The Chumaer River sub-watershed is located in the northwestern part of the SRYR, whose main channel also drains from the glaciers (Fig. 1a). There were 753 continental-type glaciers with a total area and volume of about 1276 km^2 and 1.044×10^{11} m^3 in the 1960s, respectively, according to the second glacier inventory of China (Guo et al., 2017). Given the effects of climate warming in recent decades, the total glacier area of the SRYR has been significantly reduced by about 120 km^2 from 1986 to 2009 (Sheng et al., 2009; Yao et al., 2014; Liu et al., 2016).

The SRYR may be divided into two nested watersheds based on locations of the two hydrological stations, the upper sub-watershed, featuring the Tuotuo River as the main channel (referred to as W_1), and the entire watershed with the Tongtian River as the main channel (denoted as W_2). W_1 has an area of 1.82×10^4 km^2 and its outlet is situated at the Tuotuo River hydrological station (34°13′12″ N, 92°26′37″ E) with an elevation of 4533 m a.s.l., while W_2 is the entire SRYR area and its outlet is located at the Zhimenda hydrological station (33°00′46″ N, 97°14′18″ E) with an elevation of 3800 m a.s.l. (Fig. 1a). Available hydrological data (1960–2014) for both stations were obtained from the Changjiang Hydrological Bureau of China. Affected by seasonally variable precipitation, water discharges in the SRYR are high in summer (June–September) and low in winter. The icing period is normally from November to May. October marks the beginning of relatively low water discharges during non-flood periods. Temperature and precipitation data for W_1

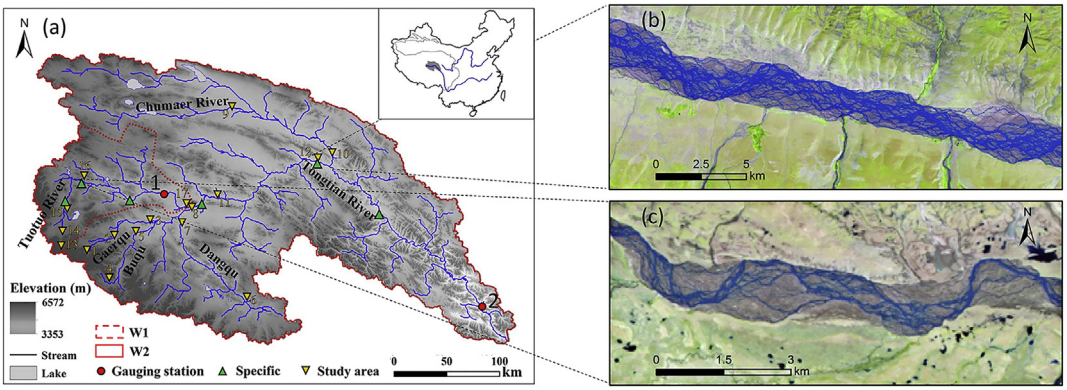

Fig. 1. Location of braided river reaches in the SRYR. (a) W_1 and W_2 are two selected nested watersheds. Points 1 and 2 are the hydrological station sites, also marking the outlet of the two watersheds. The 17 inverted triangles are selected braided reaches. The six green triangles are the selected upstream, middle, and downstream reaches along the Tuotuo and Tongtian rivers. (b) An enlarged example of the Tongtian River. (c) An enlarged example of the Tuotuo River. (For interpretation of the references to colour in this figure legend, the reader is referred to the web version of this article.)

were obtained from the Tuotuo River meteorological station, which is located at the same location as the hydrological station. Similar data for W_2 were obtained from the Qumalai meteorological station (34° 07′ 48″ N, 95° 46′ 48″ E), which is 184 km away from the Zhimenda hydrological station. Mean air temperature at these two meteorological stations is −3.78° at the Tuotuo station and 3.42 °C at the Zhimenda station. To reflect spatial diversity of morphological structures of the braided river systems, 17 braided reaches were selected along four main tributaries in the study area, the Tuotuo, Dangqu, Chumaer, and Buqu rivers, and the main channel of W_2 (i.e., the Tongtian River). The first tributary (i.e., the Tuotuo River) belongs to W_1, while the remaining tributaries are within W_2 (Fig. 1a). The selected reaches extended along each channel for about 5 km and contained no tributaries.

Remote sensing images from Landsat 4–5 TM, Landsat 7 ETM SLC-off, and Landsat 8 OLI_TRIS with 30 m spatial resolution were selected for extracting morphological information of the braided river reaches in W_1 and W_2. The selected images did not have clouds covering the focused areas within W_1 and W_2. Two types of data were obtained from them. First, 17 braided reaches distributed within W_1 and W_2 in either 2015 or 2016 were selected to represent morphological conditions in both the flood (July–September) and dry seasons (represented by October). These data were used to analyze morphological diversity and the associated spatial patterns in two different seasons. Second, images representing braided channels in the upper, middle, and lower reaches of the Tuotuo and Tongtian rivers, respectively were selected for both flood and dry seasons from 1986 to 2016 to address temporal changes of morphological structures of the braided channels in the two nested watersheds (Fig. 1a) (see detailed description of the selected images in the supplementary material).

2.2. Image processing method

The selected images were processed in ArcGIS and ENVI software following the procedure that included raster computing, clipping, classification and extraction, and channel simplification. Raster computing involved distinguishing water bodies from lands in each grid of the image based on values of an index that was calculated from the spectrum of multiple bands. McFeeters (1996) originally proposed the normalized difference water index (NDWI), which is based on the normalized ratio of the green and near-red bands, for extracting water bodies from images. The modified normalized difference water index (MNDWI) based on green and medium-red bands is an improvement of NDWI (Singh et al., 2015). Remote sensing imagery tests using different types of water bodies showed that MNDWI can more effectively reveal the characteristics of water bodies, and hence can be used to easily distinguish shadows from water bodies. Therefore, we used MNDWI in this study.

Clipping means intercepting the studied reach from the original image to exclude potential effects of non-research areas and increase the processing efficiency. This study adopted the method of grid clipping in ArcGIS and set the border of clipping area as the boundary of the river valley (about 5 km long) at each selected site (Fig. 1a). During classification extraction, areas with water were separated from other parts in terms of the threshold value of MNDWI determined in preliminary tests. For smaller channels and bars with widths <30 m, which is the resolution of the images, automatic extraction often failed and manual correction was subsequently required to reduce errors.

2.3. Braiding indices and other parameters

Four indices quantifying braiding intensity, which are $BI_B{}^*$ (bar index), BI_{T3} (channel count index), P_T (sinuosity index), and $P_T{}^*$ (sinuosity index), have been commonly used to quantitatively compare morphological similarities and differences among braided channels in different rivers (Egozi and Ashmore, 2008). $BI_B{}^*$ was a modified version of BI_B, defined as the sum of twice the length of all islands and (or) bars (L_b) in a reach divided by the length of the reach (L_r) measured along the centerline of the reach. $BI_B{}^*$ modified BI_B by adding the total number of bars (N_b) per reach length (L_r) (Brice, 1960; Germanoski and Schumm, 1993; Egozi and Ashmore, 2008):

$$BI_{B*} = 2\sum L_b/L_r + \sum N_b/L \tag{1}$$

BI_{T3} was created by Hong and Davies (1979) based on BI_{T1} of Howard et al. (1970), and expressed as the average number of branches (braids or anabranches) for each section after equidistantly dividing the river reach (Howard et al., 1970; Davies, 1987):

$$BI_{T3} = \langle N_L \rangle \tag{2}$$

where $<N_L>$ is the mean number of channels per transact across the width of a braided reach. P_T was defined as the total length of channels (ΣL_L) per unit length of river (L_r) (Hong and Davies, 1979):

$$P_T = \sum L_L/L_r \tag{3}$$

Referring to the definition of P_T, Mosley (1981) proposed $P_T{}^*$ as a variant of total sinuosity that substitutes the (straight line) reach length with the length of the main channel (ΣL_{ML}):

$$P_{T*} = \sum L_L / \sum L_{ML} \tag{4}$$

Although the two branch length indices (i.e., P_T and $P_T{}^*$) are similar, P_T actually represents the number of branches, while $P_T{}^*$ indicates the

sinuosity of the branches. Given that these indices were all defined for active branches containing water flow, inundation and exposure of the branches caused by fluctuation of water stages may be an important cause for the change of braiding intensity.

Average valley width, W_R, was defined in this study as the total area of the valley reach (S_V) divided by the length of the valley (L_V):

$$W_R = S_V / L_V \quad (5)$$

Under the same flow conditions, the laterally extending degree of braided channels in river reaches with different valley widths might not be consistent because of the influence of river valley width. Therefore, we proposed a new index, braiding density, to characterize the lateral distribution density of the branches in a given reach:

$$R_R = BI_{T3} / W_R \quad (6)$$

This index (i.e., R_R) is helpful for comparing the braiding intensity of braided rivers with different active channel widths (Peirce et al., 2018). In addition, the active water area is equally important because it is not only positively related to the associated water discharge, but also directly tied to the braiding intensity. In this study, we quantified this morphological feature by proposing the active water area ratio (R_W), defined as the ratio of surface area of the water body (S_W) to valley area (S_V):

$$R_W = S_W / S_V \quad (7)$$

2.4. Data analysis methods

Data obtained from meteorological and hydrological stations on temperature, precipitation, water discharges, and suspended sediment loads/concentrations over the study period from 1960 to 2014 for the nested watersheds (i.e., W_1 and W_2) were examined and compared between the two watersheds. For the 17 selected reaches distributed in both W_1 and W_2, the four braided indices, BI_B^*, BI_{T3}, P_T, and P_T^*, were calculated and compared among them for the wet/flood season (July–September) and dry season (October–April), respectively. The comparison allowed us to select one (i.e., BI_{T3}) for further analysis. Morphological characteristics of the 17 selected reaches and their spatial patterns between the two nested watersheds were revealed by investigating relationships between BI_{T3} and elevations, BI_{T3} and W_R, and R_R and elevations. Furthermore, morphological changes of the studied river reaches in response to variable hydrological regimes were explored for the Tuotuo and Tongtian rivers and the main channels of W_1 and W_2 (Fig. 1a) based on the data compiled for the selected upstream, middle, and downstream reaches in the 1986–2016 period. These changes were characterized in terms of the BI_{T3}-R_W and R_W-Q relationships, and the hysteresis loops between BI_{T3} and Q for all six selected reaches in the two nested watersheds.

3. Results and analyses

3.1. Temporal changes of climatic conditions and sediment load

3.1.1. Temperature, precipitation, and runoff

Morphological changes of braided channels are closely related to those of runoff (Zhang et al., 2007; Yu et al., 2014; Karmaker et al., 2017; Wu et al., 2018b). From 1960 to 2014, the average annual runoff (Q) and precipitation (P) for W_1 were 9.40×10^4 m^3 and 293.8 mm, while Q and P for W_2 were 1.325×10^6 m^3 and 489.0 mm, respectively. Although Q in W_2 was 14.1 times larger than that of W_1, the runoff coefficient (R_c), defined as the ratio of the runoff depth (mm) to P (mm), was 0.197 and 0.182 for W_2 and W_1, respectively (Fig. 2), indicating that the yield capacity of runoff per unit area is similar. Temporal trends

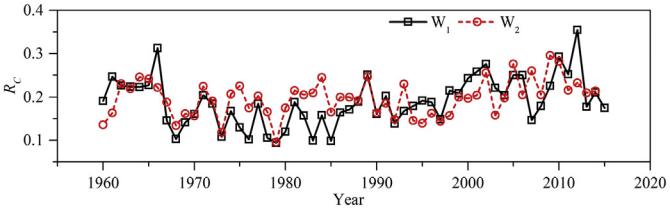

Fig. 2. Temporal changes of runoff ratio in the two nested watersheds of the SRYR from 1960 to 2014.

of R_c in W_1 and W_2 were also very similar, showing no statistically significant pattern for the entire period, but two weak decreasing and increasing trends in the 1960–1989 and 1990–2014 sub-periods (Fig. 2). The decreasing trend in the first sub-period was not significant in either W_1 or W_2. Also, the average value of R_c was 0.169 in W_1 with a coefficient of variation (CV) of 0.324; the mean R_c was 0.192 in W_2 with CV = 0.204. A two-sample different test showed that the two mean R_c values were not statistically different. Thus, from 1960 to 1989, the yield capacity remained similar both temporally and spatially. In the second sub-period from 1990 to 2014, R_c increased significantly in both W_1 and W_2 ($R^2 = 0.251$ and 0.385, respectively) with their values increased by 53.69% and 58.95% in 2014, while P only increased by 75.41% and 15.31%, respectively. The increased Q in W_1 was apparently ascribed to the increased P, but the increase of Q in W_2 cannot be simply explained by a smaller increase in P. The increased Q might be related to continuous global warming, which has caused continuous increase of air temperature (T), resulting in accelerated glacier melting (Sheng et al., 2009; Yao et al., 2014).

Averaged monthly values of T, P, and Q demonstrated similar intra-year patterns in both W_1 and W_2 (Fig. 3a and b), lower T values from November to March were associated with lower P and Q values, whereas higher T values between April and October were accompanied by higher and more variable values of P and Q. Accompanying these similarities were subtle discrepancies between W_1 and W_2. In W_1, the mean monthly peak P occurred in July, but the mean monthly peak Q was delayed one month to August (Fig. 3a), leading to much lower R_c value in July (0.193) than in August (0.276). Given that T was similar in these two months (8.22 and 7.68 °C, respectively), the differences in R_c values must be caused by factors other than land cover, which should not have drastic changes between these two months. Because W_1 is closer to glaciers, this other factor was likely glacier melting, which may start in late April and was accelerated in the subsequent months owing to the increased T and reached the highest rate in August (Fig. 3a). In W_2, the mean monthly Q reached the peak in both July and August (1086.17 and 1081.00 m^3/s, respectively), while the peak mean monthly P occurred much earlier in June (Fig. 3b). Yet R_c in June (0.128) was much less than that in July (0.223) and August (0.245). Because W_2 is much larger than W_1, the lower R_c value in June when the mean monthly P reached the peak partially reflected the fact that runoff in W_2 took a longer time to route through the larger network of channels. However, the similar mean monthly Q values in July and August strongly suggested that melted glaciers, during these two months when the mean monthly T reached its peak, supplied a sufficient amount of melt surface runoff. Thus, different patterns among the mean monthly T, P, and Q in W_1 and W_2 reflected variable interactions of the three variables over the two nested watersheds representing two different spatial scales.

3.1.2. Suspended sediment

Monthly mean suspended sediment flux (Q_s, kg/s) in W_1 and W_2 followed an annual cycle that mostly peaked in June and remained low typically from October to April (Fig. 4). The mean Q_s value in June over the entire study period was 42.04 and 651.65 kg/s for W_1 and W_2, respectively, while the mean in October was 2.14 and 71.83 kg/s for W_1 and W_2, respectively. Clearly, suspended sediment was driven by surface runoff during summer months in the nested watersheds.

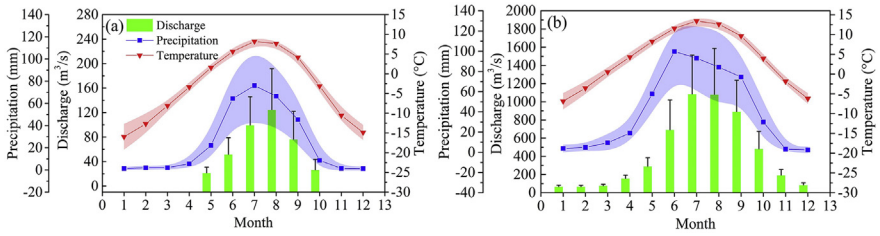

Fig. 3. Multi-year averaged monthly discharge, precipitation, and temperature in (a) W_1 watershed and (b) W_2 watershed.

The CV of Q_s in W_1 was 2.49, slightly higher than that in W_2 (2.16). This similar variation possibly suggested that suspended sediment transported in both watersheds may come from similar source areas, which could be glacier melting areas. These areas are closer to the outlet of W_1 than that of W_2 and thus the damping effect of Q_s in W_2 caused by a longer travel distance could effectively reduce Q_s variation. Furthermore, Q_s values were strongly correlated with Q in both W_1 and W_2 (Fig. 5a and b), indicating that sediment sources were relatively simple, such that no hysteresis loops existed over the entire time period. Since the river system of these nested watersheds can be characterized as gravel-bed braided rivers where storage of fine particles (e.g., sand and silt) was limited, suspended sediment transported in these channels mainly comes from glacier melting in the uplands of the contributing areas. This assertion may be further confirmed by the fact that suspended sediment concentrations (C, kg/m^3) were almost the same in both watersheds regardless of the magnitudes of the water discharges (Fig. 5c).

3.2. Morphological structures of braided channel reaches

Standardized magnitudes of the four braiding indices (i.e., I/I_{max}) for the five selected segments showed different degrees of variation during the flood season. Two of them (No. 13 and 17) had very similar I/I_{max} values, evidenced by their smaller CVs (0.112 and 0.109) (Table 1). The other three (No. 14, 15, and 16) had relatively high variations among the four indices, as their CVs were 0.341, 0.253, 0.211, respectively (Table 1). These variations were not related to the elevation of their locations (Fig. 6a). In W_2, I/I_{max} values for all selected segments were very similar except one (No. 4, upstream on Buqu River) with CV = 0.212 during the flood season, which was comparable with the one in W_1 (No. 15) (Table 1). Variation of I/I_{max} values in W_2 was independent of the elevation of their locations (Fig. 6a). Almost the same pattern of variability for I/I_{max} values prevailed during the dry season for both W_1 and W_2 (Table 1). Similarly, these variations were not correlated with the elevation of the locations of the reaches (Fig. 6b). The limited variations among the four indices in only four selected reaches (No. 4, 14, 15, and 16) indicated that the braiding intensity of a braided reach may be reasonably well characterized by any of the four tested indices. Hereafter, BI_{T3} was chosen because of its relatively clear physical meaning.

Values of BI_{T3} for all selected rivers in W_1 were well blended with those in reaches within W_2 that have elevations greater than about 4500 m (Fig. 6a and b), showing similar braiding intensities of river reaches in W_1 and W_2. The I/I_{max} values for BI_{T3} during the flood and dry seasons are centered around means of 2.24 and 2.54 with a very small CV (0.25 and 0.18), apparently indicating similar morphological characteristics among these selected reaches regardless of their location. Higher braiding intensities existed in two selected reaches in W_2 with elevations lower than 4500 m during both flood and dry seasons (No. 11 and 12 in Table 1). They are located in the middle reach of the Tongtian River (Fig. 1a) and do not have distinct physiographic conditions compared with other segments. Thus, their high braiding intensities could not be simply explained by the elevation of the reaches.

However, BI_{T3} values were strongly correlated with the averaged valley width (W_R) for both the flood and dry seasons (Fig. 7a and b). This correlation was characterized by a single positive linear relationship between BI_{T3} and W_R for all 17 reaches from the W_1 and W_2 watersheds for both seasons, suggesting that braided segments in W_1 had similar morphological features to those in W_2. Additionally, the linear relationship in the flood season was different from that in the dry season (Fig. 7a and b). In general, an increase of W_R was accompanied by a higher rate of increase in BI_{T3} during the flood season than that during the dry season. There also existed a threshold value of W_R, which was 709.5 m where the two trend lines intersect (Fig. 7a and b). In selected reaches with W_R below the threshold, BI_{T3} during the dry season was higher than that during the flood season, whereas above the threshold, the opposite case emerged. A possible explanation is as follows. In braided reaches with relatively narrow alluvial valleys, increase of water discharges from the dry to flood seasons may submerge smaller branches, leaving fewer larger branches and the main channel. In those with relatively wider alluvial valleys, similar increase of water discharges would lead to fewer submerged branches.

By definition (i.e., Eq. (6)), braiding density (R_R) eliminated the impact of valley width on morphology of the braided reaches. During the flood season, R_R decreased slightly with the increase of elevation (Fig. 8a). Nonetheless, the decreasing trend was weak and statistically insignificant. These R_R values were very similar for selected reaches in both W_1 and W_2, which was demonstrated by their similar means (0.0039 and 0.0038) and CV (0.232 and 0.276). During the dry season, R_R values were apparently not correlated with elevations of the associated reaches (Fig. 8b) and were characterized by similar means (0.0038 and 0.0037) and CV (0.231 and 0.280) for reaches in both

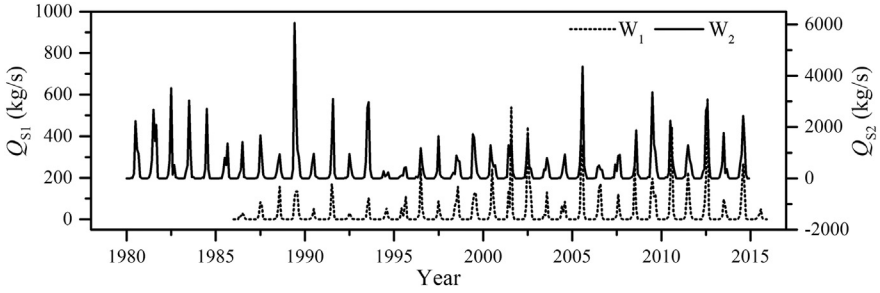

Fig. 4. Suspended sediment flux in W_1 (1985 to 2016) and W_2 watersheds (1980 to 2015).

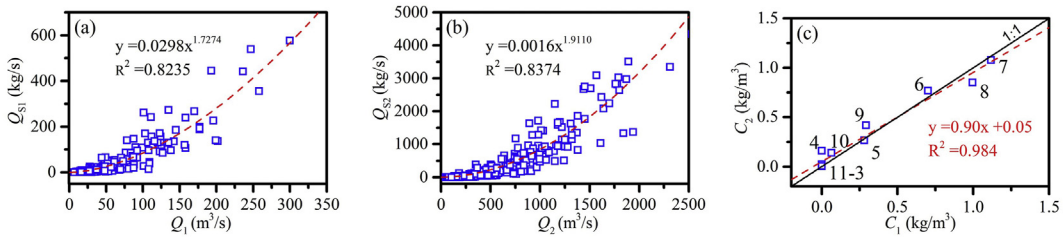

Fig. 5. Relationships between the monthly discharge and suspended sediment flux at the two hydrological stations in (a) W1 and (b) W2. (c) Comparison of average monthly sediment concentrations in the W1 and W2 watersheds (note: numbers refer to months).

watersheds. It was also worth noting that R_R values remained similar in general between flood and dry seasons regarding both their means and variations.

3.3. Morphodynamic changes of the main channels in the two nested watersheds

Dynamic responses of channel morphology along the main river of W_1 and W_2 watersheds may be reflected by morphological changes of the selected reaches upstream, middle, and downstream of the two nested watersheds (Fig. 1a). Along the main channel of W_1 (i.e., the Tuotuo River), braiding density (BI_{T3}) varied with active water area (R_w) in a similar style in all three reaches, which may be characterized by a parabolic relationship (Fig. 9a–c). This relationship indicated that as water discharges increased from the dry to flood seasons, BI_{T3} first increased and then decreased after reaching the maximum, which was 3.34, 2.13, and 3.15 in the three reaches, respectively. Furthermore, the threshold value of R_w that led to the maximum value of BI_{T3} was the same in the three reaches (0.43). Below this value, which may be featured by dry and early flood seasons when water discharges were relatively low, more channels emerged with an increase of the active water area, mainly caused by the increased water discharges. After this threshold, braiding density started to decrease possibly because of merging of smaller channels. Both increasing and decreasing rates were similar in upstream and downstream reaches, while lower in the middle reach. Clearly, morphological changes of braided structure were spatially identical along the main river, which was evidenced by the same threshold R_w value, marking the turning point of the two opposite trends of morphological changes. Very similar patterns of morphological changes occurred in the three reaches along the main channel of W_2 (i.e., the Tongtian River) (Fig. 9d–f). Values of BI_{T3} in the three reaches of W_2 were much higher than those in the three reaches of W_1, which were 12.61, 7.59, and 3.42 in the upstream, middle, and downstream reaches, respectively. However, the threshold value of R_w for BI_{T3} reaching the maximum was still about 0.43 in all three reaches, indicating that morphological responses of the main channels to their flow regimes were similar in the two nested watersheds.

Increase of R_w with water discharges (Q) followed a power function with statistical significance for all six reaches in the two watersheds (Fig. 10a and b). For W_1, the R_w - Q relationship was similar in upstream and downstream reaches, but different in the middle one (Fig. 10a). The exponents were generally less than one, suggesting that as Q became larger (e.g., the flood season), increasing Q would cause an increasingly smaller degree of increase in R_w. As R_w reached its critical value (0.43), the associated critical Q value was 88.46, 140.75, and 111.86 m^3/s, respectively. Given that the ratio of average valley width (W_R) in the upstream, middle, and downstream reach to that in the upstream was 1.00, 1.51, and 1.60, respectively, the difference of the critical Q values in the three reaches was independent of W_R and possibly more relevant to variable sizes and shapes of bars among the three reaches. The exponents of the power functions for the three reaches in W_2 were generally higher than those for the three reaches in W_1 (Fig. 10b), showing that active water areas in W_1 increased more than those in W_2 with the increase of Q values. Again, the R_w - Q relationship in the middle reach was different from that in both upstream and downstream reaches and the critical Q values for the threshold R_w were 1371.14, 955.60, and 1844.85 m^3/s, respectively, which was not consistent with their corresponding W_R values (1.00, 0.51, and 0.33 in the upstream, middle, and downstream reach, respectively).

Averaged over the entire study period, BI_{T3} demonstrated variable degrees of hysteresis loops with regard to multi-year averaged monthly mean water discharge, Q_m (Fig. 11). In W_1, all three reaches had clockwise loops for BI_{T3} (Fig. 11a–c). In the upstream reach, BI_{T3} increased

Table 1
Statistical results of the I/I_{max} (defined in Fig. 6) values for the four selected braiding indices calculated from the 17 selected braided river reaches.

No.		Elevation (m)	Flood season			Dry season		
			Mean	σ	CV	Mean	σ	CV
1	W_2	5260	0.275	0.050	0.183	0.418	0.025	0.060
2		4790	0.301	0.019	0.063	0.402	0.032	0.079
3		4593	0.273	0.039	0.144	0.440	0.043	0.098
4		5050	0.220	0.047	0.212	0.348	0.017	0.049
5		4660	0.265	0.049	0.185	0.377	0.031	0.082
6		4690	0.352	0.031	0.089	0.399	0.026	0.065
7		4525	0.277	0.053	0.190	0.388	0.046	0.117
8		4485	0.658	0.058	0.088	0.443	0.028	0.063
9		4500	0.232	0.011	0.045	0.321	0.008	0.025
10		4260	0.441	0.041	0.094	0.480	0.033	0.068
11		4440	0.970	0.027	0.028	0.960	0.022	0.023
12		4245	0.988	0.023	0.023	1.000	0.000	0.000
13	W_1	5200	0.400	0.044	0.109	0.560	0.031	0.055
14		5060	0.176	0.060	0.341	0.235	0.070	0.299
15		4756	0.219	0.046	0.211	0.329	0.035	0.107
16		4910	0.280	0.071	0.253	0.373	0.080	0.215
17		4490	0.533	0.060	0.112	0.384	0.024	0.063

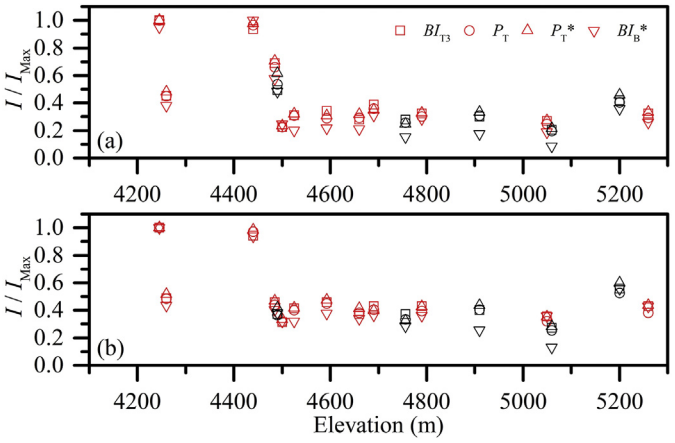

Fig. 6. Comparison of four indices in (a) the flood season (b) the dry season (The abscissa is the Lagrangian distance beginning at the Zhimenda station and calculated upstream. The ordinate is each braided intensity divided by the respective maximum value. The maximum value of BI_{T3}, P_T, P_T^* and BI_B^* in the flood season was 8.45, 10.63, 8.97, and 12.43, respectively, and in the dry season was 6.36, 8.15, 6.88, and 9.56, respectively.).

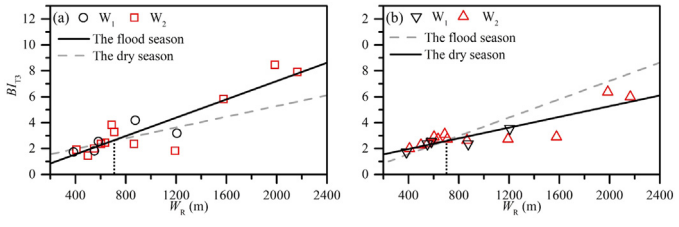

Fig. 7. Relationship between BI_{T3} and W_R for the 17 selected reaches in W_1 and W_2 during (a) the flood season (b) the dry season. The vertical dashed line represents the threshold elevation.

swiftly in June and July and decreased promptly in September after reaching the maximum in August (Fig. 11a). For the same Q_m, BI_{T3} was lower in September than in July, suggesting that the falling of water levels in smaller channel branches was faster than that in relatively larger ones, such that a few smaller branches active in July dried out quickly in September. From September to October, water discharge dropped significantly from 71 m^3/s to 21 m^3/s. Although Q_m in October was slightly higher than that in May, the BI_{T3} value in October was clearly larger than that in May, suggesting that reduction of Q_m in this braided reach did not make smaller channels dry out simultaneously. In other words, morphological responses of channels to the change of water discharges were lagged. It should be noted that similar morphological responses to the changing hydrology occurred in the middle and downstream reaches as well (Fig. 11b–c). This consistency of hysteresis loops suggested that from upstream to downstream, relatively small channel branches were more sensitive to seasonal changes of hydrological processes in W_1. In W_2, the three reaches featured different hysteresis patterns. In the upstream reach, there was essentially no loop, signifying that BI_{T3} was monotonously correlated with Q_m, and thus smaller channels responded to the changes of Q_m similar to larger channels. In the middle reach, the existing loop was very weak, such that it may be reasonably well characterized by a single relationship (Fig. 11e). Channel responses to the monthly hydrological variations were similar to those in the upstream reach. In the downstream reach, the figure-8 loop (Fig. 11f) indicated more complex channel responses to the variable hydrological processes. The complexity was primarily caused by the fact that the highest Q_m value was still lower than the critical Q (1844.85 m^3/s) for BI_{T3} reaching its maximum.

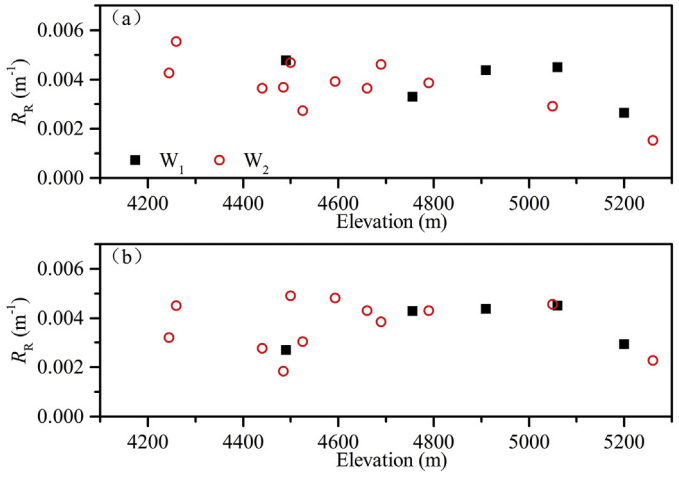

Fig. 8. Variations of braiding density, R_R with respect to their elevations for the 17 selected reaches in the (a) flood season (b) dry period (The abscissa is the Lagrangian distance, beginning at the Zhimenda station, and calculated in the upstream direction).

4. Discussion

4.1. Impacts of active valley width and runoff on braiding intensity

The active width of an alluvial valley defines the space in which braided channels may freely expand and contract in the lateral direction over a long time period (Bertoldi et al., 2009c; Werbylo et al., 2017; Peirce et al., 2018; Fryirs et al., 2019). Therefore, it actually determines the potential maximum morphological complexity and braiding intensity of active braided channel at the reach scale (Bertoldi et al., 2009c; Ashmore et al., 2011;). Our results from the 17 selected reaches confirmed the key role that the active valley width (W_R) played in controlling morphology of the braided reaches in the Source Region of Yangtze River (SRYR). The positive linear relationship between BI_{T3} and W_R (Fig. 7) is consistent with the braided systems along the middle and lower reaches of the Brahmaputra River, India, whose elevations are much lower than those in the SRYR (Sarma, 2005; Sarma and Acharjee, 2018). However, this linearity also means that braiding intensity per unit valley width (R_R) should be invariable, which was corroborated by our results (Fig. 8), suggesting the self-similarity nature of the braided systems in the SRYR. This nature has also been found in many low-elevation braided rivers (Sapozhnikov and Foufoula-Georgiou, 1996; Walsh and Hicks, 2002; Sambrook Smith et al., 2005; Kelly, 2006; An et al., 2013). Because the 17 selected reaches were distributed across both W_1 and W_2 watersheds, the self-similarity is apparently homogenous in space.

Temporal changes of the morphological structure of the braided reaches in the SRYR were influenced by the dominant impact of water discharges on braiding intensity (BI_{T3}). Recent studies in flume experiments and field investigations at shorter temporal scales (e.g., instantaneous or event scales) have shown that braiding intensity is positively correlated with discharge, stream power, and bedload (Bertoldi et al., 2009c; Ashmore et al., 2011; Peirce et al., 2018). Our results demonstrated the lumped effect of these variables at longer temporal scales (annual and decade scales). The braiding intensity can reach the maximum at an intermediate water discharge during a given flood event (Bertoldi et al., 2010; Lotsari et al., 2018; Wu et al., 2018b). This observation was sustained over the period of more than three decades in our study (Fig. 9). Furthermore, along the Tuotuo and Tongtian rivers in both W_1 and W_2, the maximum braiding intensity always occurred at the stage when surface water area was about 40% of the valley width (Fig. 9a–f), showing spatially homogeneous response of morphological structure to the change of flow conditions.

Variations of water discharges at shorter temporal scales directly drive the dynamic processes of bar exposure and inundation (Zanoni et al., 2008), which simultaneously alter amplitudes of braiding intensity in many low-elevation braided rivers (Bertoldi et al., 2010; Middleton et al., 2018; Schuurman et al., 2018). At longer temporal scales, as in our study, the lumped effect of these processes emerged in the nested smaller watershed (W_1), which was represented by the strong hysteresis loops in all three selected reaches along the Tuotuo River, the main channel of W_1 (Fig. 11a–c). Although daily discharges in June and July were generally comparable to those in September (Fig. 3a), the former led to higher magnitudes of BI_{T3} values than the latter, suggesting that the similar effect of variable daily discharges on braiding intensity remained in multi-year monthly averaged discharges. Moreover, the general clockwise loops in the relationship between BI_{T3} and Q_m (Fig. 11a–c) suggested that after peak flows, which typically occurred in August (Fig. 4), braided rivers in W_1 tended to be less complex, which is the opposite of the response of braided rivers to discharge variation at shorter time scales (Marra et al., 2014; Redolfi et al., 2016). However, at the larger spatial scale (W_2), this effect was not evident because no, or very weak, hysteresis loops were observed in the three selected reaches along the Tongtian River (Fig. 11d–f). This difference between W_1 and W_2 watersheds revealed that the temporally lumped effect of hydrological processes on morphology of braided rivers varies at different spatial scales.

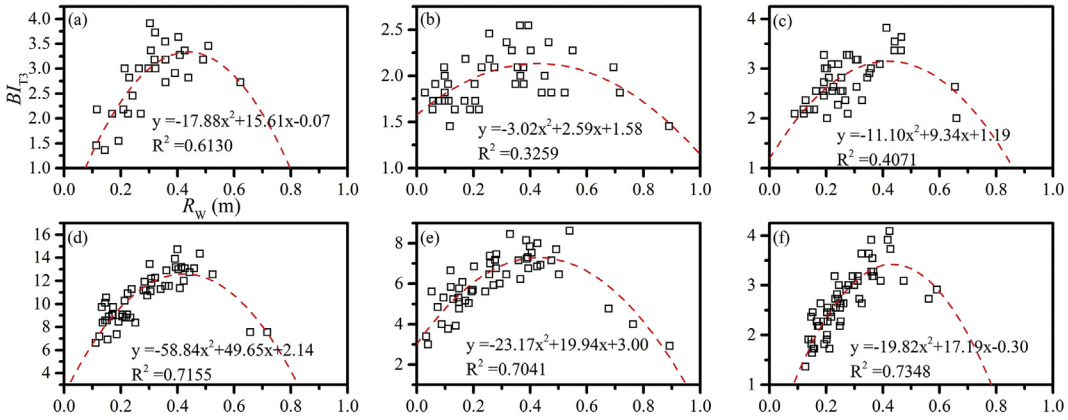

Fig. 9. Relationships between braiding index BI_{T3} and water area ratio R_w in the (a) upstream (b) middle (c) downstream reaches of W_1 and the (d) upstream (e) middle (f) downstream reaches of W_2.

The similar positive R_W and Q relationships for all selected reaches between W_1 and W_2 (Fig. 10) suggested that the surface area of a braided reach was less sensitive than braiding intensity for capturing morphodynamic characteristics of braided rivers, thus BI_{T3} or R_R should be used preferentially to describe the morphological structure of a braided reach. A limitation of morphological analysis at longer temporal scales may be highlighted by its attenuation effect, which was generally displayed in all hysteresis loops (Fig. 11a–f). Although water discharges were the highest in August, the associated braiding intensity was not the highest, despite the earlier finding that branches tend to increase significantly after peak floods (Egozi and Ashmore, 2009; Bertoldi et al., 2010; Schuurman et al., 2018).

4.2. Inference of the possible impact of sediment load on channel morphology

Morphology of braided rivers and its change over time are directly affected by bedload transported through the channels (Ashmore, 1988; Young and Davies, 1991; Bertoldi et al., 2009a; Williams et al., 2015). Unfortunately, no bedload data were available in the braided rivers within the SRYR because the harsh physical conditions (e.g., long and cold winter and very high elevations (>4000 m)) and difficult access to these remote locations made direct measurement of bedload extremely difficult, if not impossible. Although suspended sediment loads transported in these braided rivers may not be directly related to the morphological structure of these braided rivers, they can still be used to infer bedload characteristics because it is well known that in large, deep rivers, bedload is about 5 to 25% of suspended load (Simons and Senturk, 1992; Turowski et al., 2010). A very interesting finding in our study was that suspended sediment concentrations (C) were always similar in the two nested watersheds (W_1 and W_2) (Fig. 5c), suggesting that suspended sediment transported at one (small) scale is proportional to that at another (larger) scale, which is different from the transport processes of suspended sediment in many low-elevation watersheds (Cammeraat, 2002; Van Dijk and Bruijnzeel, 2005; de Vente et al., 2007; Moreno-de las Heras et al., 2010). This finding was also supported by the fact that the two sediment rating curves (SRC) had very similar exponents (1.717 for W_1 and 1.911 for W_2) (Fig. 5a and b). Given that the Qinghai-Tibet Plateau has experienced continuous temperature increase caused by the global warming effect (Zhang et al., 2015; Wu et al., 2018a; Gao et al., 2019; Pritchard, 2019), glaciers in the source area of W_1 have been subject to increased melting (Sheng et al., 2009; Yao et al., 2014; Liu et al., 2016). The similar values of the exponents in the two SRCs suggested that increased glacier melting has not supplied additional suspended sediment to the braided river systems. A plausible implication is that bedload might not be affected by glacier melting either, which could explain the spatially ubiquitous self-similarity of morphological structures in the 17 selected braided reaches and the three selected reaches along the two main channels.

Moreover, the two SRCs have exponents greater than one, suggesting that both watersheds tend to be transport limited and transport capacity increased as discharges increased (Hickin, 1995; Asselman, 2000). Over the entire study period (1960–2014), the flood season (which mainly contains July, August, and September) on average transported 84.5 and 78.8% of the annual total suspended load. This suggests that sediment transport is dominated by precipitation (P) that occurred in the flood season, which can be evidenced by the strong linear relationship between C and P in both watersheds (Fig. 12). The braided rivers in the SRYR are typical gravel-bedded channels. The rainfall-driven suspended sediment transport at capacity implies that suspended sediment was not stored in the braided rivers during high flows; Therefore, the trend of increasing braiding density with water discharges in all three reaches along the two main channels (i.e., the Tuotuo and Tongtian rivers) (Fig. 10) was mainly controlled by morphology of gravel bars possibly less affected by limited suspended sediment transport.

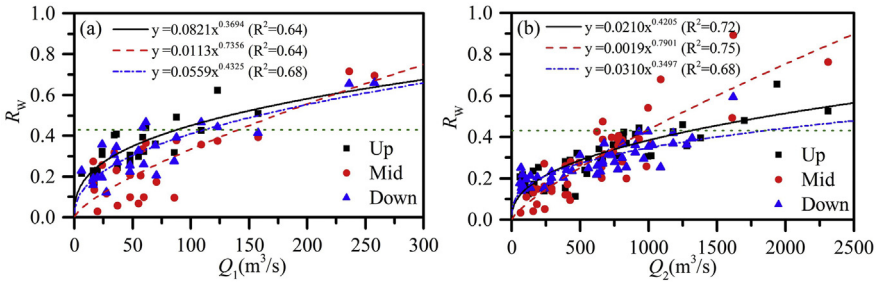

Fig. 10. Relationship between water area ratio R_W and Q in (a) W_1 and (b) W_2.

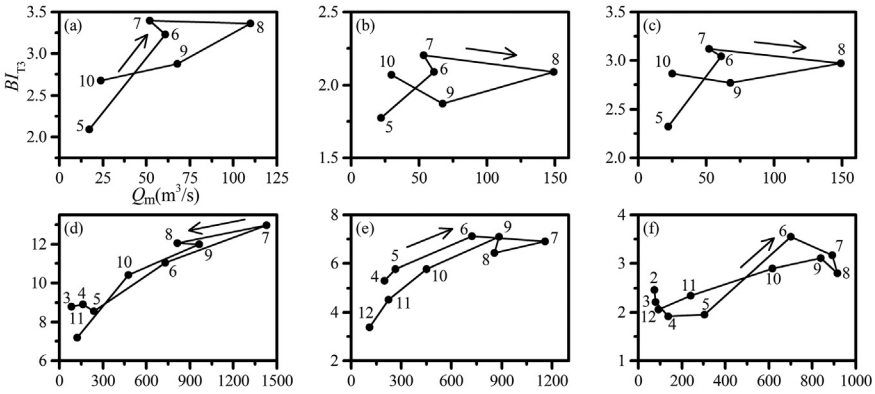

Fig. 11. Hysteresis loops of monthly averaged BI_{T3} and Q_m in the (a) upstream (b) middle (c) downstream reaches of W_1 and the (d) upstream (e) middle (f) downstream reaches of W_2 (numbers along the loops refer to the associated months).

5. Conclusions

Braided rivers in the Source Region of the Yangtze River (SRYR) have unique physiographic settings featuring very high elevations and glacier sources. Their morphological structures and spatial and temporal changes of these structures have not been studied thus far. We examined them using selected braided reaches distributed within the two nested watersheds (W_1 and W_2). Our results led to the following conclusions:

(1) Braiding intensity and active valley width are two fundamental morphological parameters in braided rivers. Although four different braiding indices exist (BI_B^*, BI_{T3}, P_T, and P_T^*), the ability to characterize the features of a braided river was similar. We suggested use of BI_{T3} because of its clearer physical meaning. Subsequent analysis for BI_{T3} revealed that braiding density per unit valley width remained similar over all selected braided reaches distributed within the two nested watersheds, showing spatially similarity of the braiding structure in braided reaches with variable valley widths. This implies that morphological structures of braided rivers in the SRYR might be similar in different locations of the entire river system. Therefore, further in-depth exploration of the fluvial processes in a single braided reach (e.g., the Tuotuo River) may allow us to generalize the results to other braided river systems in the SRYR.

(2) At longer temporal scales (e.g., annual and decadal scales), braiding density always reached the maximum with a medium magnitude of flow regardless of locations along the two main channels of the nested watersheds. Seasonal variable water discharges could cause different braiding densities for two months with similar mean discharges (i.e., hysteresis loops between braiding density and monthly mean water discharges). Although this morphodynamic feature is consistent with dynamic control of instantaneous and variable discharges on bar sizes and shapes at the smaller temporal scales, it disappeared with the increase of spatial scales from W_1 to W_2. This revealed that the cumulative effect of hydrological processes on morphological features of braided rivers varied over time and space. It also highlighted the challenge of fully understanding fluvial processes dominating morphological structures of braided rivers and their evolution.

(3) Suspended sediment in the braided rivers within the SRYR was generally transported at capacity and mostly transported through the rivers during the wet seasons (i.e., July, August, and September). The transported load was proportional from a small spatial scale (i.e., W_1) to a large one (i.e., W_2), suggesting that (i) increased glacier melting did not significantly increase sediment supply to the braided rivers, and (ii) suspended sediment was not stored in braided channels and/or within gravel bars. Possible inference from findings of suspended sediment transport on bedload might be that bedload transport was generally limited, such that it was inadequate to significantly change sizes and shapes of gravel bars and subsequently braiding characteristics of channels.

This study provided the first set of information on morphological composition of braided rivers with very high elevations and its temporal and spatial responses to variable water discharges on the Qinghai-Tibet Plateau. While our findings demonstrated some similarities and discrepancies with braided rivers in other regions of the world, these findings were at longer temporal scales. Further investigation based on high-resolution morphological data and hydrological data at finer temporal scales are needed to better understand morphodynamic and hydrodynamic processes driving changes of braided rivers in the SRYR at variable spatial scales in the context of climate change.

Supplementary data to this article can be found online at https://doi.org/10.1016/j.geomorph.2019.106945.

Declaration of competing interest

The authors declare that they have no known competing financial interests or personal relationships that could have appeared to influence the work reported in this paper.

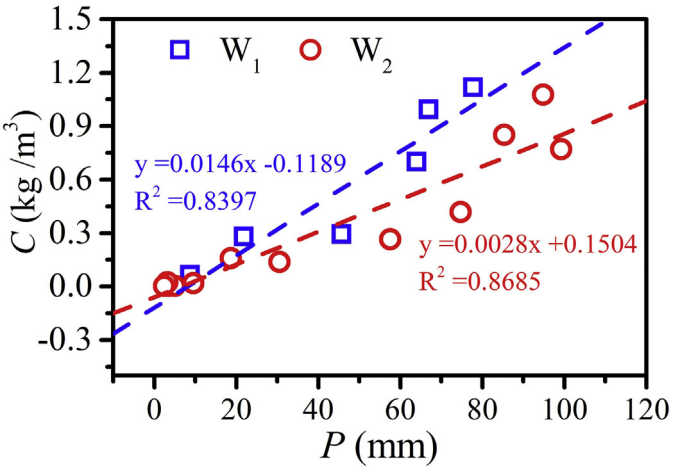

Fig. 12. Linear relationships between suspended sediment concentration and precipitation for W_1 and W_2.

Acknowledgments

This study was supported by the National Natural Science Foundation of China (91647118, 51709020, 91647204, 51979012) and Overseas Expertise Introduction 111 Project for Discipline Innovation (D18013). We thank Yezhou Wu, Xu Yan, and Hanyuan Yang for field survey and data processing. We also thank two anonymous referees for their constructive comments and suggestions that have improved the quality of the paper.

References

An, H.P., Chen, S.C., Chan, H.C., Hsu, Y., 2013. Dimension and frequency of bar formation in a braided river. Inter. J. Sediment Res. 28, 358–367.
An, C., Moodie, A.J., Ma, H., Fu, X., Zhang, Y., Naito, K., Parker, G., 2018. Morphodynamic model of the lower Yellow River: flux or entrainment form for sediment mass conservation? Earth Surf. Dynamics 6, 989–1010.
Ashmore, P.E., 1982. Laboratory modelling of gravel braided stream morphology. Earth Surf. Process. Landf. 7, 201–225.
Ashmore, P.E., 1988. Bed load transport in braided gravel-bed stream models. Earth Surf. Process. Landf. 13, 677–695.
Ashmore, P.E., 1991. How do gravel-bed rivers braid? Can. J. Earth Sci. 28, 326–341.
Ashmore, P., Bertoldi, W., Tobias Gardner, J., 2011. Active width of gravel-bed braided rivers. Earth Surf. Process. Landf. 36, 1510–1521.
Asselman, N.E.M., 2000. Fitting and interpretation of sediment rating curves. J. Hydrol. 234, 228–248.
Baki, A.B.M., Gan, T.Y., 2012. Riverbank migration and island dynamics of the braided Jamuna River of the Ganges–Brahmaputra basin using multi-temporal Landsat images. Quarter. International 263, 148–161.
Bakker, M., Antoniazza, G., Odermatt, E., Lane, S.N., 2019. Morphological response of an alpine braided reach to sediment-laden flow events. J. Geophys. Res. Earth Surf. 124, 1310–1328.
Bertoldi, W., Tubino, M., 2007. River bifurcations: experimental observations on equilibrium configurations. Water Resour. Res. 43. https://doi.org/10.1029/2007WR005907.
Bertoldi, W., Ashmore, P., Tubino, M., 2009a. A method for estimating the mean bed load flux in braided rivers. Geomorphology 103, 330–340.
Bertoldi, W., Gurnell, A., Surian, N., Tockner, K., Zanoni, L., Ziliani, L., Zolezzi, G., 2009b. Understanding reference processes: linkages between river flows, sediment dynamics and vegetated landforms along the Tagliamento River. Italy. River Res. Appl. 25, 501–516.
Bertoldi, W., Zanoni, L., Tubino, M., 2009c. Planform dynamics of braided streams. Earth Surf. Process. Landf. 34, 547–557.
Bertoldi, W., Zanoni, L., Tubino, M., 2010. Assessment of morphological changes induced by flow and flood pulses in a gravel bed braided river: the Tagliamento River (Italy). Geomorphology 114, 348–360.
Bertoldi, W., Drake, N.A., Gurnell, A.M., 2011. Interactions between river flows and colonizing vegetation on a braided river: exploring spatial and temporal dynamics in riparian vegetation cover using satellite data. Earth Surf. Process. Landf. 36, 1474–1486.
Bertoldi, W., Welber, M., Mao, L., Zanella, S., Comiti, F., 2014. A flume experiment on wood storage and remobilization in braided river systems. Earth Surf. Process. Landf. 39, 804–813.
Blue, B., Brierley, G., Yu, G.-a., 2013. Geodiversity in the Yellow River source zone. J.Geogr. Sci. 23, 775–792.
Brice, J.C., 1960. Index of description of channel braiding. Geol. Soc.Am. Bull. 71, 1833.
Brice, J.C., 1964. Channel patterns and terraces of the Loup Rivers in Nebraska. Geological Survey Professional Paper 422-D.
Cammeraat, L.H., 2002. A review of two strongly contrasting geomorphological systems within the context of scale. Earth Surf. Process. Landf. 27, 1201–1222.
Carling, P.A., Trieu, H., Hornby, D.D., Huang, H.Q., Darby, S.E., Sear, D.A., Hutton, C., Hill, C., Ali, Z., Ahmed, A., Iqbal, I., Hussain, Z., 2018. Are equilibrium multichannel networks predictable? The case of the regulated Indus River, Pakistan. Geomorphology 302, 20–34.
Chalov, S.R., Alexeevsky, N.I., 2015. Braided rivers: structure, types and hydrological effects. Hydrol. Res. 46, 258–275.
Connor-Streich, G., Henshaw, A.J., Brasington, J., Bertoldi, W., Harvey, G.L., 2018. Let's get connected: a new graph theory-based approach and toolbox for understanding braided river morphodynamics. Wiley Interdiscip. Rev. Water 5, e1296.
Cook, K.L., 2017. An evaluation of the effectiveness of low-cost UAVs and structure from motion for geomorphic change detection. Geomorphology 278, 195–208.
Coulthard, T.J., 2005. Effects of vegetation on braided stream pattern and dynamics. Water Resour.s Res. 41. doi:https://doi.org/10.1029/2004WR003201.
Davies, M.R.B., 1987. Problems of bed load transport in braided gravel-bed rivers. In: Bathurst, J.C., Hey, R.D. (Eds.), C.R. Thorne. Sediment Transport in Gravel-bed Rivers, Wiley, Chichester, pp. 793–828.
Dubey, A.K., Gupta, P., Dutta, S., Kumar, B., 2014. Evaluation of satellite-altimetry-derived river stage variation for the braided Brahmaputra River. Inter. J. Remote Sens. 35, 7815–7827.
Egozi, R., Ashmore, P., 2008. Defining and measuring braiding intensity. Earth Surf. Process. Landf. 33, 2121–2138.
Egozi, R., Ashmore, P., 2009. Experimental analysis of braided channel pattern response to increased discharge. J. Geophs. Res. Earth Surf., 114 https://doi.org/10.1029/2008JF001099.
Friend, P.F., Sinha, R., 1993. Braiding and meandering parameters. Geol. Soc. Special Publication 75, 105–111.
Fryirs, K.A., Wheaton, J.M., Bizzi, S., Williams, R., Brierley, G.J., 2019. To plug-in or not to plug-in? Geomorphic analysis of rivers using the River Styles Framework in an era of big data acquisition and automation. Wiley Interdiscip. Rev. Water 6, e1372. https://doi.org/10.1002/wat2.1372.
Gao, C., Liu, L., Ma, D., He, K., Xu, Y.P., 2019. Assessing responses of hydrological processes to climate change over the southeastern Tibetan Plateau based on resampling of future climate scenarios. Sci. Total Envir. 664, 737–752.
Germanoski, D., Schumm, S.A., 1993. Changes in braided river morphology resulting from aggradation and degradation. J.Geol. 101, 451–466.
Gogoi, P., 2018. Landscape Evolution Modelling in Large, Complex Braided River the Brahmaputra: A Case Study of Majuli Island, North-East India. PhD, University of Nottingham, UK.
Gran, K., Paola, C., 2001. Riparian vegetation controls on braided stream dynamics. Water Resour. Res. 37, 3275–3283.
Gran, K.B., Tal, M., Wartman, E.D., 2015. Co-evolution of riparian vegetation and channel dynamics in an aggrading braided river system, Mount Pinatubo, Philippines. Earth Surf. Process. Landf. 40, 1101–1115.
Guerit, L., Barrier, L., Liu, Y., Narteau, C., Lajeunesse, E., Gayer, E., Métivier, F., 2018. Uniform grain-size distribution in the active layer of a shallow, gravel-bedded, braided river (the Urumqi River, China) and implications for paleo-hydrology. Earth Surf. Dynam. 6, 1011–1021.
Guo, W., Liu, S., Xu, J., Wu, L., Shangguan, D., Yao, X., Wei, J., Bao, W., Yu, P., Liu, Q., Jiang, Z., 2017. The second Chinese glacier inventory: data, methods and results. J. Glaciol. 61, 357–372.
Hickin, E.J., 1995. River Geomorphology. John Wiley & Sons, Chichester.
Hong, L.B., Davies, T.R.H., 1979. A study of stream braiding: Summary. Geol. Soc. Am. Bull. 90, 1094–1095.
Howard, A.D., Keetch, M.E., Vincent, C.L., 1970. Topological and geometrical properties of braided streams. Water Resour. Res. 6, 1674–1688.
Huber, E., Huggenberger, P., 2015. Morphological perspective on the sedimentary characteristics of a coarse, braided reach: Tagliamento River (NE Italy). Geomorphology 248, 111–124.
Hundey, E.J., Ashmore, P.E., 2009. Length scale of braided river morphology. Water Resour. Res. 45. https://doi.org/10.1029/2008WR007521.
Javernick, L., Redolfi, M., Bertoldi, W., 2018. Evaluation of a numerical model's ability to predict bed load transport observed in braided river experiments. Advanc. Water Res. 115, 207–218.
Karmaker, T., Dutta, S., 2011. Erodibility of fine soil from the composite river bank of Brahmaputra in India. Hydrol. Process. 25, 104–111.
Karmaker, T., Hmanta, M., Subashisa, D., 2017. Study of channel instability in the braided Brahmaputra river using satellite imagery. Curr. Sci. 112, 1533–1543.
Kelly, S., 2006. Scaling and hierarchy in braided rivers and their deposits_ examples and implications for reservoir modelling. In: J.L.B. Gregory H. Sambrook Smith, Charlie S. Bristow and Geoff E. Petts (Ed.), Braided Rivers: Process, Deposits, Ecology and Management. John Wiley & Sons, Chichester, UK.
Li, Z.W., Wang, Z.Y., Pan, B.Z., Zhu, H.L., Li, W.Z., 2014. The development mechanism of gravel bars in rivers. Quarter. International 336, 73–79.
Li, Z.W., Yu, G.A., Brierley, G., Wang, Z.Y., 2016. Vegetative impacts upon bedload transport capacity and channel stability for differing alluvial planforms in the Yellow River source zone. Hydrol. Earth Sys. Sci. 20, 3013–3025.
Li, J., Xia, J., Zhou, M., Deng, S., Zhang, X., 2017a. Variation in reach-scale thalweg migration intensity in a braided reach of the lower Yellow River in 1986–2015. Earth Surf. Process.Landf. 42, 1952–1962.
Li, Z.W., Yu, G.A., Brierley, G.J., Wang, Z.Y., Jia, Y.H., 2017b. Migration and cutoff of meanders in the hyperarid environment of the middle Tarim River, northwestern China. Geomorphology 276, 116–124.
Liu, Z., Yao, Z., Wang, R., 2016. Contribution of glacial melt to river runoff as determined by stable isotopes at the source region of the Yangtze River. China. Hydrol. Res. 47, 442–453.
Lotsari, E.S., Calle, M., Benito, G., Kukko, A., Kaartinen, H., Hyyppä, J., Hyyppä, H., Alho, P., 2018. Topographical change caused by moderate and small floods in a gravel bed ephemeral river – a depth-averaged morphodynamic simulation approach. Earth Surf. Dynami. 6, 163–185.
Marra, W.A., Kleinhans, M.G., Addink, E.A., 2014. Network concepts to describe channel importance and change in multichannel systems: test results for the Jamuna River, Bangladesh. Earth Surf. Process. Landf. 39, 766–778.
McFeeters, S.K., 1996. The use of the Normalized Difference Water Index (NDWI) in the delineation of open water features. Inter. J. Remote Sens. 17, 1425–1432.
Métivier, F., Devauchelle, O., Chauvet, H., Lajeunesse, E., Meunier, P., Blanckaert, K., Ashmore, P., Zhang, Z., Fan, Y., Liu, Y., Dong, Z., Ye, B., 2016. Geometry of meandering and braided gravel-bed threads from the Bayanbulak Grassland, Tianshan, P. R. China. Earth Surf. Dynami. 4, 273–283.
Middleton, L., Ashmore, P., Leduc, P., Sjogren, D., 2018. Rates of planimetric change in a proglacial gravel-bed braided river: field measurement and physical modeling. Earth Surf. Process. Landf. 44, 752–765.
Moreno-de las Heras, M., Nicolau, J.M., Merino-Martín, L., Wilcox, B.P., 2010. Plot-scale effects on runoff and erosion along a slope degradation gradient. Water Resour. Res., 46 https://doi.org/10.1029/2009WR007875.
Mosley, M.P., 1981. Semi-determinate hydraulic geometry of river channels, South Island, New Zealand. Earth Surf. Process. Landf. 6, 137.
Nicholas, A., 2013. Morphodynamic diversity of the world's largest rivers. Geology 41, 475–478.
Pearson, E., Smith, M.W., Klaar, M.J., Brown, L.E., 2017. Can high resolution 3D topographic surveys provide reliable grain size estimates in gravel bed rivers? Geomorphology 293, 143–155.

Peirce, S., Ashmore, P., Leduc, P., 2018. The variability in the morphological active width: results from physical models of gravel-bed braided rivers. Earth Surf. Process. Landf. 43, 2371–2383.
Pritchard, H.D., 2019. Asia's shrinking glaciers protect large populations from drought stress. Nature 569, 649–654.
Redolfi, M., Tubino, M., Bertoldi, W., Brasington, J., 2016. Analysis of reach-scale elevation distribution in braided rivers: definition of a new morphologic indicator and estimation of mean quantities. Water Resour. Res. 52, 5951–5970.
Rusnák, M., Sládek, J., Kidová, A., Lehotský, M., 2018. Template for high-resolution river landscape mapping using UAV technology. Measurement 115, 139–151.
Rust, B.R., 1972. Structure and process in a braided river. Sedimentol. 18, 221–245.
Rust, B.R., 1978. A classification of alluvial channel systems. Canadian Soc. Petroleum Geologists, Memoir 5, 187–198.
Sambrook Smith, G.H., Ashworth, P.J., Best, J.L., Woodward, J., Simpson, C.J., 2005. The morphology and facies of sandy braided rivers- some considerations of scale invariance. Spec. Publs int. Ass. Sediment. 35, 145–158.
Sambrook Smith, G.H., Ashworth, P.J., Best, J.L., Woodward, J., Simpson, C.J., 2006. The sedimentology and alluvial architecture of the sandy braided South Saskatchewan River, Canada. Sedimentol. 53, 413–434.
Sapozhnikov, V., Foufoula-Georgiou, E., 1996. Self-affinity in braided rivers. Water Resour. Res. 32, 1429–1439.
Sarma, J.N., 2005. Fluvial process and morphology of the Brahmaputra River in Assam, India. Geomorphology 70, 226–256.
Sarma, J., Acharjee, S., 2018. A study on variation in channel width and braiding intensity of the Brahmaputra River in Assam, India. Geosci. 8, 343.
Schuurman, F., Kleinhans, M.G., Middelkoop, H., 2016. Network response to disturbances in large sand-bed braided rivers. Earth Surf. Dynam. 4, 25–45.
Schuurman, F., Ta, W., Post, S., Sokolewicz, M., Busnelli, M., Kleinhans, M., 2018. Response of braiding channel morphodynamics to peak discharge changes in the Upper Yellow River. Earth Surf. Process. Landf. 43, 1648–1662.
Sheng, Y.P., Wang, G.Y., Wang, G.X., Pu, J.C., Wang, X., 2009. Impacts of climate change on glacial water resources and hydrological cycles in the Yangtze River source region, the Qing-Tibetan Plateau. China: A progress report. Sci. Cold Arid Reg. 1, 475–495.
Simons, D.B., Senturk, F., 1992. Sediment Transport Technology: Water and Sediment Dynamics. Water Resources Publications, Littleton, USA.
Singh, K.V., Setia, R., Sahoo, S., Prasad, A., Pateriya, B., 2015. Evaluation of NDWI and MNDWI for assessment of waterlogging by integrating digital elevation model and groundwater level. Geocarto International 30, 650–661.
Storz-Peretz, Y., Laronne, J.B., Surian, N., Lucía, A., 2016. Flow recession as a driver of the morpho-texture of braided streams. Earth Surf. Process. Landf. 41, 754–770.
Sun, J., Lin, B.-l., Kuang, H.-w., 2015a. Numerical modelling of channel migration with application to laboratory rivers. Inter. J. Sediment. Res. 30, 13–27.
Sun, J., Lin, B., Yang, H., 2015b. Development and application of a braided river model with non-uniform sediment transport. Adv. Water Resour. 81, 62–74.
Surian, N., Fontana, A., 2017. The Tagliamento River: The Fluvial Landscape and Long-Term Evolution of a Large Alpine Braided River. In: M.M. Soldati M. (Ed.), Landscapes and Landforms of Italy. Springer, Cham.
Tal, M., Paola, C., 2010. Effects of vegetation on channel morphodynamics: results and insights from laboratory experiments. Earth Surf. Process. Landf. 35, 1014–1028.
Turowski, J.M., Rickenmann, D., Dadson, S.J., 2010. The partitioning of the total sediment load of a river into suspended load and bedload: a review of empirical data. Sedimentol. 57, 1126–1146.
Unsworth, C.A., Nicholas, A.P., Ashworth, P.J., Simpson, C.J., Best, J.L., Lane, S.N., Parsons, D.R., Sambrook Smith, G.H., 2016. Using bedform migration and orientation to infer sediment transport pathways in a sandy braided river. In: Dan Hanes, M.G., Constantinescu, George (Eds.), The International Conference on Fluvial Hydraulics (River Flow 2016). CRC Press/Balkema, St. Louis, United States.
Van Dijk, A.I.J.M., Bruijnzeel, L.A.S., 2005. Key controls and scale effects on sediment budgets: recent findings in agricultural upland Java, Indonesia. International Symposium on Sediment Budgets, International Association of Hydrological Sciences (IAHS). IAHS-AISH publication, Foz do Iguaco, Brazil, pp. 24–31.
Vázquez-Tarrío, D., Borgniet, L., Liébault, F., Recking, A., 2017. Using UAS optical imagery and SfM photogrammetry to characterize the surface grain size of gravel bars in a braided river (Vénéon River, French Alps). Geomorphology 285, 94–105.
de Vente, J., Poesen, J., Arabkhedri, M., Verstraeten, G., 2007. The sediment delivery problem revisited. Progr. Phys. Geogr.: Earth and Envir. 31, 155–178.
Walsh, J., Hicks, D.M., 2002. Braided channels: Self-similar or self-affine? Water Resour. Res.38, 18–1–18-16. doi:https://doi.org/10.1029/2001WR000749.
Wang, Z., Li, Z., Xu, M., Yu, G., 2016. River Morphodynamics and Stream Ecology of the Qinghai-Tibet Plateau. CRC Press, Taylor & Francis Ltd, Netherland.
Welber, M., Bertoldi, W., Tubino, M., 2012. The response of braided planform configuration to flow variations, bed reworking and vegetation: the case of the Tagliamento River, Italy. Earth Surf.Process. Landf. 37, 572–582.
Werbylo, K.L., Farnsworth, J.M., Baasch, D.M., Farrell, P.D., 2017. Investigating the accuracy of photointerpreted unvegetated channel widths in a braided river system: a Platte River case study. Geomorphology 278, 163–170.
Wheaton, J.M., Brasington, J., Darby, S.E., Kasprak, A., Sear, D., Vericat, D., 2013. Morphodynamic signatures of braiding mechanisms as expressed through change in sediment storage in a gravel-bed river. J. Geophys. Res. Earth Surf. 118, 759–779.
Williams, R.D., Brasington, J., Vericat, D., Hicks, D.M., 2014. Hyperscale terrain modelling of braided rivers: fusing mobile terrestrial laser scanning and optical bathymetric mapping. Earth Surf. Process. Landf. 39, 167–183.
Williams, R.D., Rennie, C.D., Brasington, J., Hicks, D.M., Vericat, D., 2015. Linking the spatial distribution of bed load transport to morphological change during high-flow events in a shallow braided river. J. Geophys. Res. Earth Surf. 120, 604–622.
Williams, R.D., Brasington, J., Hicks, D.M., 2016a. Numerical modelling of braided river morphodynamics: review and future challenges. Geogra. Compass 10, 102–127.
Williams, R.D., Measures, R., Hicks, D.M., Brasington, J., 2016b. Assessment of a numerical model to reproduce event-scale erosion and deposition distributions in a braided river. Water Resour.Res. 52, 6621–6642.
Wu, T., Qin, Y., Wu, X., Li, R., Zou, D., Xie, C., 2018a. Spatiotemporal changes of freezing/thawing indices and their response to recent climate change on the Qinghai-Tibet Plateau from 1980 to 2013. Theor. Applied Climatol. 132, 1187–1199.
Wu, X., Li, Z., Gao, P., Huang, C., Hu, T., 2018b. Response of the downstream braided channel to Zhikong Reservoir on Lhasa River. Water 10, 1144.
Xu, J., 1997. Study of sedimentation zones in a large sand-bed braided river: an example from the Hanjiang River of China. Geomorphology 21, 153–165.
Yao, Z.J., Liu, Z.F., Huang, H.Q., Liu, G.H., Wu, S.S., 2014. Statistical estimation of the impacts of glaciers and climate change on river runoff in the headwaters of the Yangtze River. Quarter. Inter. 336, 89–97.
Young, W.J., Davies, T.R.H., 1991. Bedload transport processes in a braided gravel-bed river model. Earth Surf. Process. Landf. 16, 499–511.
Yu, G.A., Liu, L., Li, Z.W., Li, Y.F., Huang, H.Q., Brierley, G., Blue, B., Wang, Z.Y., Pan, B.Z., 2013. Fluvial diversity in relation to valley setting in the source region of the Yangtze and Yellow Rivers. J. Geogra. Sci. 23, 817–832.
Yu, G.A., Brierley, G., Huang, H.Q., Wang, Z., Blue, B., Ma, Y., 2014. An environmental gradient of vegetative controls upon channel planform in the source region of the Yangtze and Yellow Rivers. Catena 119, 143–153.
Yu, G.A., Disse, M., Huang, H.Q., Yu, Y., Li, Z.W., 2016. River network evolution and fluvial process responses to human activity in a hyper-arid environment - case of the Tarim River in Northwest China. Catena 147, 96–109.
Yu, G.A., Li, Z.W., Disse, M., Huang, H.Q., 2017. Sediment dynamics of an allogenic river channel in a very arid environment. Hydrol. Process. 31, 2050–2061.
Zanoni, L., Gurnell, A., Drake, N., Surian, N., 2008. Island dynamics in a braided river from analysis of historical maps and air photographs. River Res. Appl. 24, 1141–1159.
Zhang, D.D., 1998. Geomorpholoigcal problems of the middle reaches of the Tsangpo River. Tibet. Earth Surf. Process. Landf. 23, 889–903.
Zhang, Y., Liu, S., Xu, J., Shangguan, D., 2007. Glacier change and glacier runoff variation in the Tuotuo River basin, the source region of Yangtze River in western China. Environ. Geol. 56, 59–68.
Zhang, Y., Su, F., Hao, Z., Xu, C., Yu, Z., Wang, L., Tong, K., 2015. Impact of projected climate change on the hydrology in the headwaters of the Yellow River basin. Hydrol. Process. 29, 4379–4397.